Engineering Structures 235 (2021) 112062

Contents lists available at ScienceDirect

Engineering Structures

journal homepage: www.elsevier.com/locate/engstruct

A geometrically defined stiffness contact for finite element models of wood joints

B. Iraola [a,*], J.M. Cabrero [a], M. Basterrechea-Arévalo [a], J. Gracia [b]

[a] Wood Chair. Department of Building Construction, Services and Structures, University of Navarra, Pamplona 31 080, Spain
[b] Department of Construction and Manufacturing Engineering, University of Oviedo, Oviedo 33 003, Spain

ARTICLE INFO

Keywords:
Stiffness contact
Wood
Joint
Solid mechanics
Finite element model

ABSTRACT

Finite element models tend to overestimate the actual elastic response of structural timber connections. The paper shows how such overprediction relates to the modelling of the contact between fasteners and timber. The use of a control parameter called stiffness contact is proposed. After an experimental campaign, a method to determine it, based only on the geometry of a rectangular contact area, is proposed. The modeling adequacy is demonstrated by applying it to dowel embedment and moment resistant wood joint tests. The obtained results show good agreement with the experimental test series.

1. Introduction

The use of timber in construction has experienced an important increase during the last years, with some representative examples of tall structures [1,2].

Since connections play a major role in the elastic response of such structures, an accurate modeling technique is of utmost importance, in which the different relevant parameters are adequately introduced and considered to obtain a realistic result. The use of advanced modelling techniques such as Finite Element Models (FEM) is mostly required to gather an improved understanding of the structural response.

In the case of structural timber connections with dowel-type fasteners, the contact between the different elements is the basis of load transfer and structural response, since the load is transferred through pressure. Moreover, due to the complexity of timber as a material, the modeling of contact becomes even more relevant. The structural behaviour of a connection is mostly defined by its stiffness (relation between the displacement and the force applied to the connection) and strength.

1.1. Modeling techniques

Regarding the stiffness, several authors have reported how that predicted by the numerical 3D FEM model of the connection is much higher than the experimental one [4,5]. Due to the usual non-linear response of timber connections, code standards provide different definitions to get a simplified linear response to develop an elasto-plastic model. For example, in Europe, such stiffness is defined as K_{ser}, and obtained from the 10% - 40% load range [6] of the testing procedure described in the European standard EN-26891 [3], whose load path is shown in Fig. 1a. It is divided in three different ranges: preloading (up to 40% of the estimated failure load (F_{est}), unloading (down to 10% of the failure load), and loading (until failure of the specimen), Fig. 1a. Although the loading procedure originates from the limitations of old testing equipment, nevertheless it allows to study in detail the response of the connection on different loading scenarios.

In the experimental response (Fig. 1b), there is an initial adjustment zone, in which the stiffness progressively increases, mainly due to adjustments. It is a widely known behavior that is usually ignored with no further consequences, since it does not play a major role in structural behaviour, where the response after this initial phase is considered (when the load is higher than 10%).

A stiffness increase is observed in comparison to the preloading phase in both unloading and loading phases. Such stiffness increase is also present in other materials [7,8]. In the case of wood, it has been attributed to a plastic deformation that occurs in a thin layer of material located in the contact surface. Dorn [5] described the appearance of non-recoverable plastic deformations, mainly on the contact surface of the wood. It is assumed to be related to the material heterogeneity at a microscopical level, and the appearance of microcracks and local compression [9]. It may not only depend on the material itself but also on the cutting tool that created the surface [10]. Additionally, moisture

* Corresponding author.
E-mail address: bisaenz@unav.edu (B. Iraola).

https://doi.org/10.1016/j.engstruct.2021.112062
Received 2 November 2020; Received in revised form 22 January 2021; Accepted 11 February 2021
Available online 27 February 2021

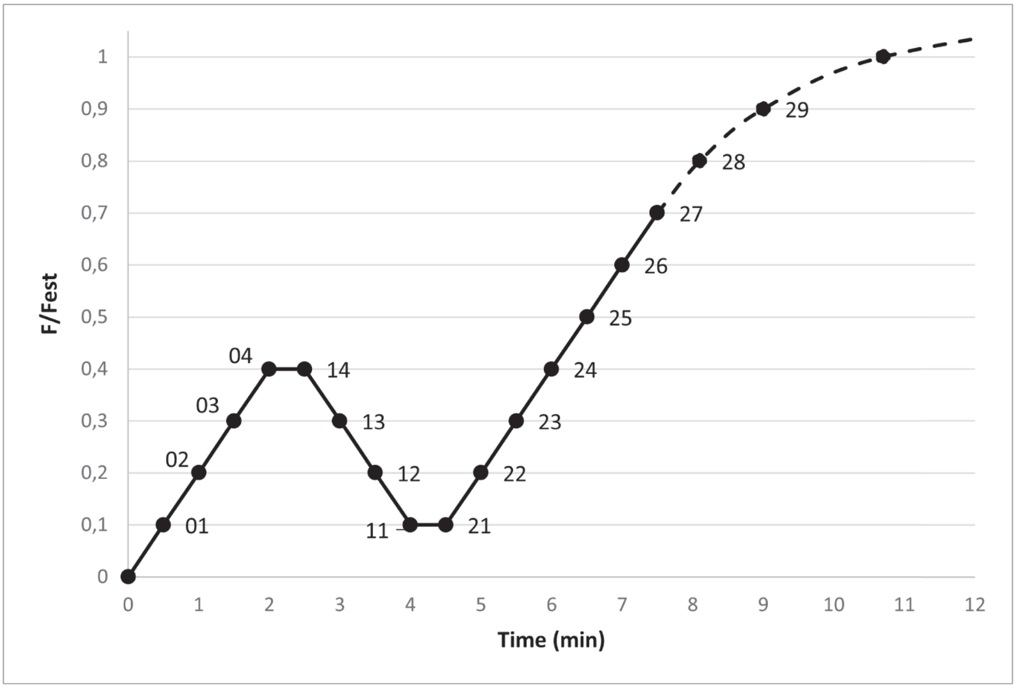

(a) Loading procedure for testing with unloading and reloading described in EN-26891 [3].

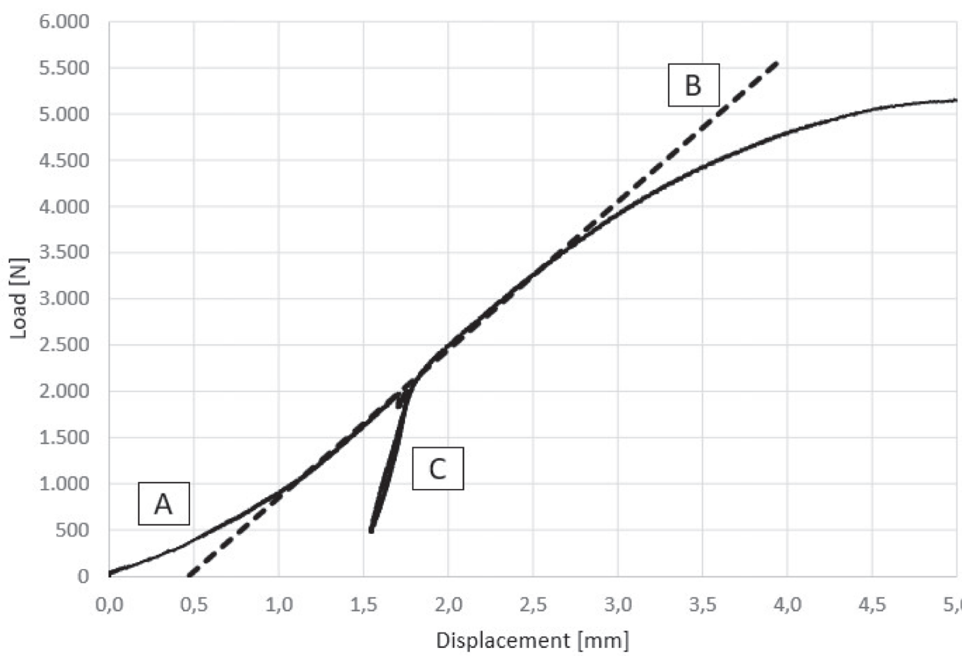

(b) Example of the typical behaviour of specimens when applying the EN26891 [3] standard loading protocol: the initial adjustments (A), the stiffness of the test (B) and the different stiffness observed in the unloading and loading phases (C).

Fig. 1. Standard load test procedure according to EN-26891 [3].

variations also influence the contact response [11,12].

However, the obtained global response results in a lower stiffness than expected from the material properties, as proved by the elastic response obtained from FEM [4,5]. This is a common issue related again with the local behaviour of the contact area. Sandhaas [4] indicates the necessity to include softening rules to recreate the stiffness of timber joints. ASTM-D143 [9] recommends to lower the elastic and shear modulus of the elements around the contact areas. A reduction of 83% is proposed for the longitudinal elastic modulus among other reductions. Hong [13] introduced a modeling method capable of accounting for wood crushing behavior to solve the wrong assumption that the behavior of the contact area follows the conventional mechanical properties of wood determined through uniaxial compression tests.

Instead of modeling a different material in the contact area, as an alternative method to obtain from modeling the overall stiffness observed in tests, the models may include a dedicated pressure-overclosure relationship in the contact surface. This modified contact interaction, called stiffness contact [14], simulates the behavior of a softened contact allowing certain penetration for the applied pressure in the contact area.

Table 1
Geometry of the tested specimens, and experimental results (density, ultimate load and corresponding strength).Missing density values correspond to testing campaigns in which this was property was not measured; missing ultimate load and strength correspond to specimens where they could not be precisely measured.

Specimen	Height [mm]	Base A [mm]	Base B [mm]	Density [kg m^3]	Slenderness	Ultimate load [N]	Strength [N/mm^2]
A1.1	25	25	25		1,0	26041	41,7
A1.2	25	25	25		1,0	28900	46,2
A2.1	50	25	25		2,0	25466	40,7
A2.2	50	25	25		2,0	28300	45,3
A3.1	75	25	25		3,0	27416	43,9
A3.2	75	25	25		3,0	30100	48,2
A4.1	100	25	25		4,0	29063	46,5
A4.2	100	25	25		4,0	25000	40,0
A5.1	125	25	25		5,0	28535	45,7
A5.2	125	25	25		5,0	29500	47,2
A6.1	150	25	25		6,0	29721	47,6
A6.2	150	25	25		6,0	26400	42,2
B1	45	45	45		1,0	89888	44,4
B2	90	45	45		2,0	90856	44,9
B3	135	45	45		3,0	89539	44,2
B4	180	45	45		4,0	81036	40,0
B5	225	45	45		5,0	85420	42,2
B6	270	45	45		6,0	82600	40,8
C1.1	150	47	29		5,2		
C1.2	150	47	29		5,2		
C1.3	150	47	29		5,2		
C1.4	150	47	29		5,2		
C2.1	75	47	29		2,6		
C2.2	75	47	29		2,6		
C2.3	75	47	29		2,6		
C2.4	75	47	29		2,6		
D1.1	169	47	29	386	5,8	57964	42,5
D1.2	169	47	29	440	5,8	53578	39,3
D1.3	169	47	28	409	6,0	57500	43,7
D2.1	319	47	29	439	11,0	49699	36,5
D2.2	319	47	27	485	11,8	32519	25,6
D2.3	319	47	28	400	11,4	40749	31,0
E1.1	134	42	47	451	3,2	81469	41,3
E1.2	134	47	48	432	2,9	85429	37,9
E1.3	135	45	44	439	3,1	86031	43,4
E1.4	133	44	44	438	3,0	79021	40,8
E2.1	270	45	44	435	6,1	83299	42,1
E2.2	270	45	44	431	6,1	80314	40,6
E2.3	270	44	43	476	6,3	79723	42,1
E2.4	271	46	47	438	5,9	76352	35,3
F1.1	132	44	46	458	3,0	83367	41,2
F1.2	128	42	45	502	3,0	64862	34,3
F1.3	128	42	44	500	3,0	62845	34,0
F1.4	133	44	44	438	3,0	67561	34,9

1.2. Analytical formulations

Previous studies have determined the stiffness contact for different materials under cylindrical indenters. In these cases, the stiffness contact is defined by [7,15]

$$SC_{ind} = \frac{dF}{d(\delta)} = \frac{2}{\sqrt{\pi}}\sqrt{A}E_r \tag{1}$$

where F is the load applied, δ is the indentation depth, A is the area, and E_r is defined as

$$E_r = \frac{E}{1-\nu^2} \tag{2}$$

where E, is the modulus of elasticity and ν is the Poisson's ratio. In the case that the indenter itself has finite elastic constants, then

$$\frac{1}{E_r} = \frac{1-\nu_s^2}{E_s} + \frac{1-\nu_i^2}{E_i} \tag{3}$$

where the subscript s refers to the specimen and subscript i to the indenter.

With these equations, Pharr et al. [7] analyzed the contact between a rigid, axisymmetric punch and an elastic half space to show the simple relationship among the contact stiffness, the contact area, and the elastic modulus that is not dependent on the geometry of the punch and Yang [15] formulated the stiffness contact only as a function of the contact area for flat-ended cylindrical indenters.

Other approaches to the stiffness contact parameter have been made: i.e., Troyon [16] proposed a generalized equation between elastic indentation and load that approximates the analytical solution very closely and can be easily fit to the experimental data. They deduce the normalized stiffness contact parameter as:

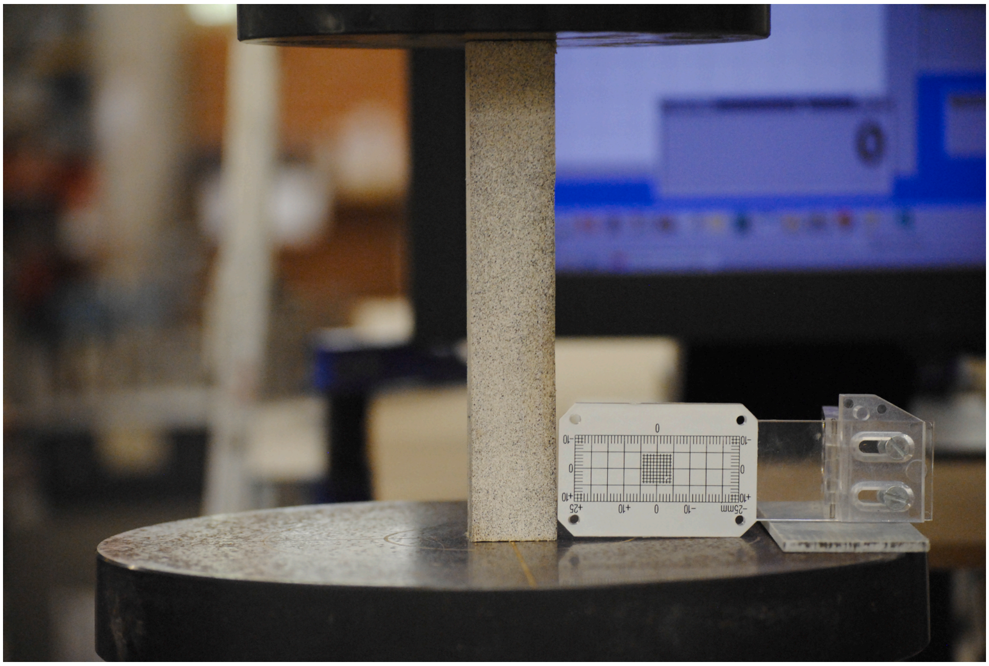

Fig. 2. Experimental setup of the tests performed in the Universidad de Navarra.

$$\overline{k}_N = \frac{k_N}{\left(\pi\gamma K^2 R^2\right)^{1/3}}, \tag{4}$$

where k_N is the contact stiffness defined as the force divided by the deformation and γ, K, and R are the interfacial energy, the reduced elastic modulus, and the curvature radius, respectively.

1.3. Foundation modulus of timber

Approaches regarding contact between dowel-type fasteners and timber often rely on the Embedment Stiffness and an Elastic Foundation [17,18].

Mirdad and Chui [19] calculated the embedment stiffness (defined in N/mm^3) with the following equation:

$$K_h = \frac{S}{dt}\left[N/mm^3\right] \tag{5}$$

where S is the load–displacement slope at 10–40%, d is the outer diameter of the screw, and t is the width of the specimen. In their model, the elastic foundation is implemented using the embedment stiffness as the foundation modulus, which results in a theoretically derived correction factor for the embedment stiffness modulus.

Reynolds et al. [20] proposed an analytical model based on [21,22], where the foundation modulus is calculated based on a complex stress function for the timber in the embedment and the friction between the dowel and the timber. The mean modulus obtained from the model for the smallest vibration is 145 kN/mm for the parallel direction, which coincides with the mean modulus obtained from the experimental data.

Yurrita and Cabrero [23] and Lemaitre et al. [24,25] used for their analytical models the values from Hwang and Komatsu [26], where not only the stiffness was measured, but the effective elastic foundation was analysed to take into account the effect of different Modulus of Elasticity. The stiffness value increases as the contact area decreases (a relation which will be discussed below).

1.4. Structure of the paper

In this paper, the influence of the contact behavior of wood on the stiffness of structural joints with dowel-type fasteners and members is analysed by means of an experimental campaign, and a formulation for its use as contact stiffness in FE models is proposed, which results in a similar formulation to Eq. (1). The paper is organized as follows: In this Section 1, the state of the art is presented, Section 2 describes the materials and methods used for the testing campaigns, Section 3 shows the results of the tests, Section 4 explains the analysis of the results, Section 5 shows the good agreement obtained for the implementation of the stiffness contact in different scenarios and finally Section 6 exposes the obtained conclusions.

2. Materials and methods

2.1. Experimental setup

To study the contact behaviour of wood, different series of compression tests were performed at the Universities of Navarra and Oviedo. The test setup followed the requirements given in EN-408 [6] to get the parallel-to-grain compression strength and the modulus of elasticity. Additionally, the unloading and reloading process are described in Fig. 1a [3] is also applied to analyse the different response at each range.

The standard specimens defined in EN-408 [6] are rectangular sections with a slenderness $\lambda = 6$, defined as $\lambda = \frac{H}{L}$, where H is the height of the specimen and L the minimum side length. Specimens maintain the same cross section in all their height, and the flat contact areas are parallel between them while perpendicular to the specimen axis, which corresponds to the fiber direction.

The given slenderness $\lambda = 6$ in the standard was taken in the presented test campaign as an established maximum limit in which second-order effects such as buckling are assumed to be avoided, so that the specimen's response is related only to material crushing. As a result, it was expected that any observed difference in behaviour would relate only to contact-related phenomena. The specimens varied in height, with slenderness mostly ranging from $\lambda = 1$ up to 6, as described in Table 1. Some specimens (series D2) feature higher slenderness to verify the validity of the assumption of avoidance of second-order effects. Fig. 2 shows the experimental setup.

The loading cycle followed the standard described in [3], shown in Fig. 1a, and described above in three different phases: preloading,

Table 2
Load-deformation response of the tested specimens. Missing data is due to unprecise recordad data from the tests. Values in brackets show the obtained coefficient of variation for similar specimens.

Specimen	Preload stiff. $K_{preload}$ [N/mm]	Unload stiff. K_{unload} [N/mm]	Load stiff. K_{load} [N/mm]	Ultimate load F_{ult} [N]	Apparent MOE E_{app} [N/mm^2]	Actual MOE E_0 [N/mm^2]	SC (E = 11 000) SC_{11} [N/mm^3]	SC (actual E) SC_E [N/mm^3]	St.Contact (15) $SC_{cal,A}$ [N/mm^3]	St.Contact (16) $SC_{cal,B}$ [N/mm^3]
A1.1	27132	34457	28943	26041	1085	11081	95	96	104	84
A1.2	28500	37600	37000	28900	1140	11796	102	101	104	84
Mean	(0,03) 27816	(0,06) 36028	(0,17) 32972	(0,07) 27470	(0,04) 1113	(0,04) 11439	(0,05) 98	(0,03) 99	(0) 104	(0) 84
A2.1	21795	27780	20441	25466	1744	11844	83	82	104	91
A2.2	25300	32700	31600	28300	2024	10781	99	100	104	91
Mean	(0,11) 23547	(0,12) 30240	(0,30) 26020	(0,07) 26883	(0,11) 1884	(0,07) 11313	(0,13) 91	(0,14) 91	(0) 104	(0) 91
A3.1	20692	25388	23383	27416	2483	10345	86	87	104	99
A3.2	24200	28800	30700	30100	2904	11960	105	102	104	99
Mean	(0,11) 22446	(0,09) 27094	(0,19) 27042	(0,07) 28758	(0,11) 2694	(0,10) 11153	(0,15) 95	(0,12) 95	(0) 104	(0) 99
A4.1	20879	26986	24838	29063	3341	12433	96	91	104	106
A4.2	20000	24900	22700	25000	3200	9706	90	95	104	106
Mean	(0,03) 20440	(0,06) 25943	(0,06) 23769	(0,11) 27032	(0,03) 3270	(0,17) 11070	(0,04) 93	(0,03) 93	(0) 104	(0) 106
A5.1	21408	26093	25558	28535	4282	12515	112	104	104	114
A5.2	23200	26200	28100	29500	4640	11615	128	124	104	114
Mean	(0,06) 22304	(0) 26147	(0,07) 26829	(0,02) 29017	(0,06) 4461	(0,05) 12065	(0,09) 120	(0,12) 114	(0) 104	(0) 114
A6.1	24017	26664	25748	29721	5764	12647	161	141	104	122
A6.2	19000	24300	22200	26400	4560	10319	104	109	104	122
Mean	(0,16) 21509	(0,07) 25482	(0,10) 23974	(0,08) 28061	(0,16) 5162	(0,14) 11483	(0,31) 133	(0,18) 125	(0) 104	(0) 122
Mean	(0,13) 23010	(0,15) 28489	(0,18) 26768	(0,06) 27870	(0,48) 3097	(0,08) 11420	(0,21) 105	(0,16) 103	(0) 104	(0,14) 103
B1	52693	57885	65917	89888	1171	12971	58	57	58	46
B2	46058	52493	55964	90856	2047	12237	56	55	58	51
B3	45080	48482	54160	89539	3005	15306	61	55	58	55
B4	39508	43268	44859	81036	3512	10470	57	59	58	59
B5	41314	45025	45149	85420	4590	11776	70	67	58	63
B6	36941	41836	40911	82600	4925	10530	66	69	58	68
Mean	(0,13) 43599	(0,13) 48165	(0,18) 51160	(0,05) 86557	(0,45) 3209	(0,15) 12215	(0,10) 61	(0,10) 60	(0) 58	(0,14) 57
C1.1	39000	56000			4292		94		72	72
C1.2	45000	56000			4952		120		72	72
C1.3	37000	45000			4072		86		72	72
C1.4	44600	53800			4908		118		72	72
Mean	(0,10) 41400	(0,10) 52700			(0,10) 4556		(0,16) 105		(0) 72	(0) 72
C2.1									72	62
C2.2	47900	62700			2636		92		72	62
C2.3	45300	69000			2493		86		72	62
C2.4	58500	76000			3219		121		72	62
Mean	(0,14) 50567	(0,10) 69233			(0,14) 2782		(0,19) 100		(0) 72	(0) 62
D1.1	34694	43046	40903	57964	4302	12558	84	77	72	75
D1.2	34387	43623	40640	53578	4264	17096	82	67	72	75
D1.3	34376	42978	40915	57500	4415	17726	87	70	74	77
Mean	(0,01) 34486	(0,01) 43215	(0) 40819	(0,04) 56347	(0,02) 4327	(0,18) 15793	(0,04) 84	(0,07) 71	(0,01) 73	(0,01) 76
D2.1	25449	29738	28336	49699	5956	14056	81	65	72	96
D2.2	20532	25942	21590	32519	5161	13585	61	52	76	101
D2.3	23920	31528	27771	40749	5798	21187	77	50	74	98
Mean	(0,11) 23300	(0,10) 29069	(0,14) 25899	(0,21) 40989	(0,07) 5639	(0,26) 16276	(0,15) 73	(0,14) 56	(0,03) 74	(0,03) 98
E1.1	44027	58239	54640	81469	2989	14327	61	56	59	56
E1.2	43465	56910	54194	85429	2582	14451	50	47	55	51
E1.3	45141	58756	56325	86031	3078	11745	63	62	58	56
E1.4	42230	55705	53415	79021	2901	15156	59	54	59	56
Mean	(0,03) 43716	(0,02) 57403	(0,02) 54644	(0,04) 82988	(0,07) 2887	(0,11) 13920	(0,10) 59	(0,11) 55	(0,03) 58	(0,04) 55

(continued on next page)

Table 2 (*continued*)

Specimen	**Preload stiff.** $K_{preload}$ [N/mm]	**Unload stiff.** K_{unload} [N/mm]	**Load stiff.** K_{load} [N/mm]	**Ultimate load** F_{ult} [N]	**Apparent MOE** E_{app} [N/mm^2]	**Actual MOE** E_0 [N/mm^2]	**SC** (E = 11 000) SC_{11} [N/mm^3]	**SC (actual** E) SC_E [N/mm^3]	**St.Contact (15)** $SC_{cal.A}$ [N/mm^3]	St.Contact (16) $SC_{cal.B}$ [N/mm^3]
E2.1	36440	44339	42680	83299	4969	13251	67	59	58	69
E2.2	36117	44774	42995	80314	4925	10443	66	69	58	69
E2.3	34970	42722	40999	79723	4990	12618	68	61	60	71
E2.4	34600	42773	40657	76352	4337	12477	53	49	56	65
Mean	(0,02) 35532	(0,02) 43652	(0,03) 41833	(0,04) 79922	(0,07) 4805	(0,10) 12197	(0,11) 63	(0,13) 60	(0,03) 58	(0,04) 68
F1.1	44261	55757	53170	83367	2887	14792	59	54	58	55
F1.2	43407	50956	46902	64862	2940	11678	63	61	60	57
F1.3	38645	52822	48592	62845	2677	11511	55	54	60	57
F1.4	39669	50462	48088	67561	2725	10776	54	55	59	56
Mean	(0,07) 41495	(0,05) 52499	(0,06) 49188	(0,13) 69659	(0,04) 2807	(0,15) 12189	(0,07) 58	(0,05) 56	(0,02) 59	(0,02) 56

unloading, and loading. The load ratios which define each phase are based on the estimated maximum load of the specimen, F_{est}, which was obtained based on the characteristic compression strength for the corresponding strength class (C24) of the Spruce specimens EN-338 [27]. This strength class, which is assigned 24N/mm^2 as its bending strength, is representative for several softwood species [28], such as *Abies alba*, *Picea Abies* or *Pinus pinaster*. During the preloading phase, the specimens are loaded up to 40% of the estimated capacity ($0.4F_{est}$). They are then unloaded up to $0.1F_{est}$ (unloading phase), to be then loaded until failure (loading phase). The load application rate is kept constant. At every change of loading phase, the load is kept constant for 30s before initializing the following (see Fig. 1a).

A Ibertest STIB 200 loading rig was used for the tests done in the Universidad de Navarra and a MTS 810 machine for those done in the Universidad de Oviedo. A ball joint was used in one of the sides to avoid moments and in the other a 40mm thick steel plate was used for load transfer. All tests were analysed with the Video Correlation Software GOM [29]. A Nikon D3000 camera and a JAI Go-5000 M-USB camera were employed for the different test series in Pamplona, with an image frequency of 1 Hz and an Aramis 5 M acquisition system equipped with two 23 mm cameras (frequency 1 Hz) in Oviedo.

2.2. Wood specimens

Clear wood spruce specimens obtained from elements graded as C24 according to EN-1912 [28] were tested under compression in the longitudinal direction. The specimens were conditioned at 22 °C and 65% relative humidity, so that the wood moisture content was 12%. The density of the different specimens was measured, and it is given in Table 1.

Specimens of series A, B, and C were obtained from the same timber element. Afterwards, to complete the testing campaign, series D, E, and F, which were obtained from a different timber element, were tested to replicate some of the specimens of the previous series. Different geometries were analysed, as shown in Table 1, with cross sections in various sizes and shapes (rectangular and square), and slenderness ranging from $\lambda = 1$ up to $\lambda = 11.8$, being the typical slenderness for most of the specimens $\lambda \leqslant 6$.

Series A, B, E, and F had square cross sections. All of them were 45 × 45 mm, except series A, which was 25 × 25 mm. The slenderness ranged

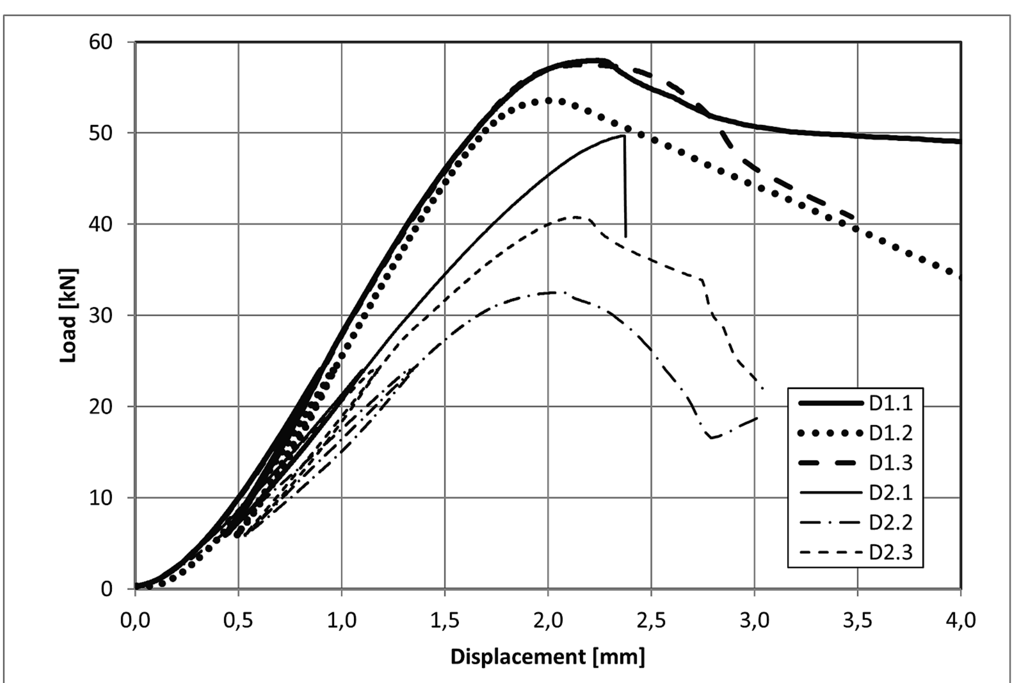

Fig. 5. Load-deformation response of test series D1 and D2.

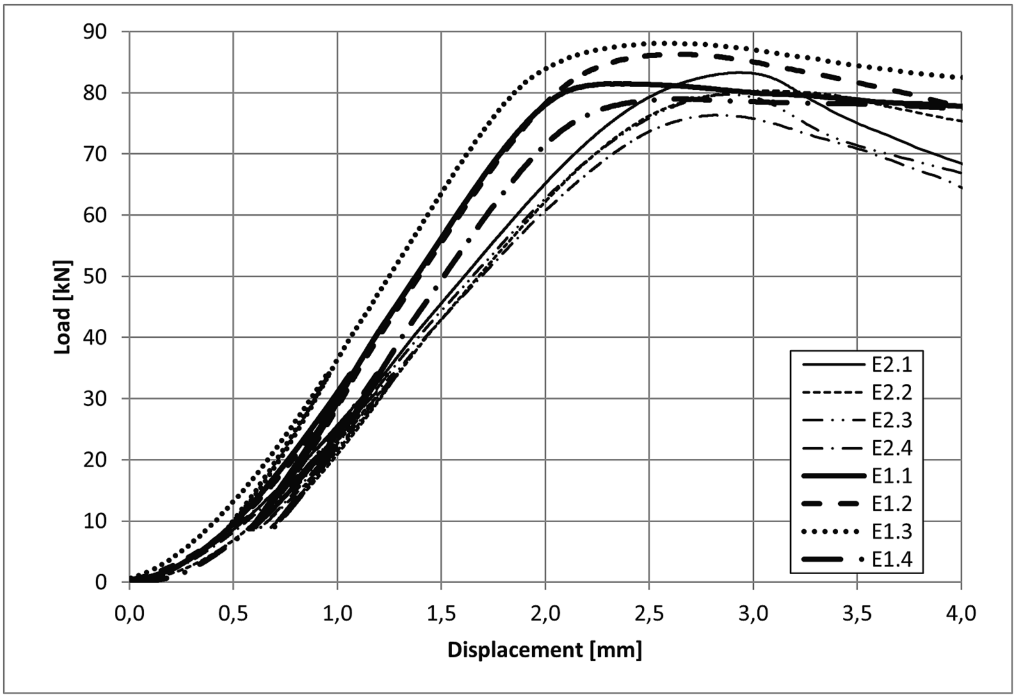

Fig. 6. Load-deformation response of test series E1 and E2.

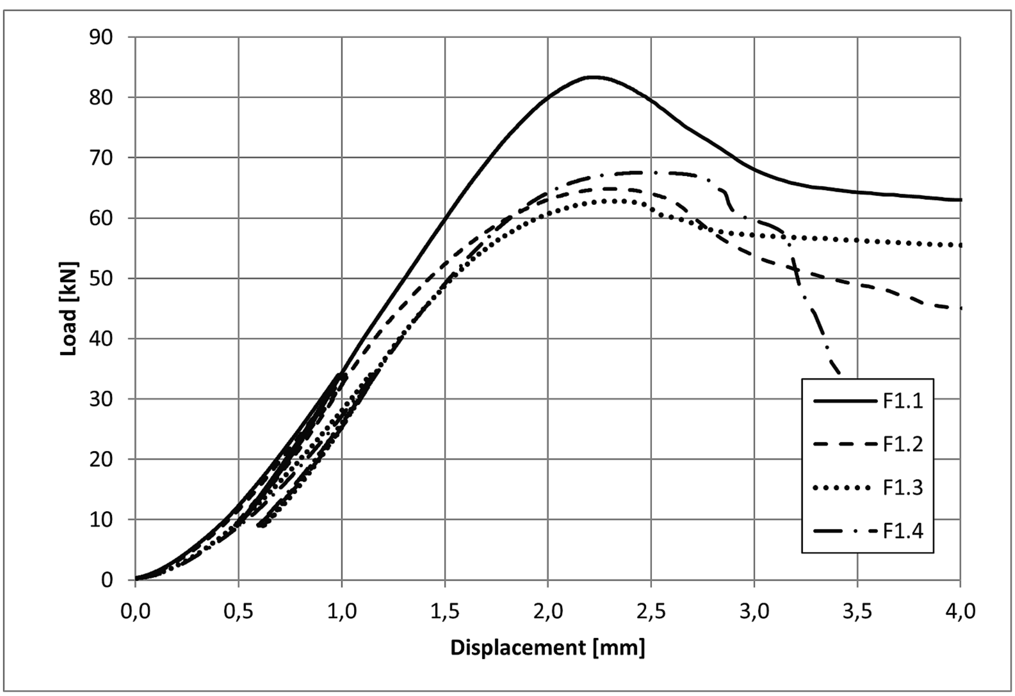

Fig. 7. Load-deformation response of test series F1.

from $\lambda = 1$ up to $\lambda = 6$. Two series, C and D, had rectangular cross sections, which were 45 × 30 mm. The slenderness referred to the minimum side length was 2.5 and 5 in series C1 and C2, and 5.6 and 10.6 in series D1 and D2, respectively.

Specimens of Series D have the same cross section as Series C (47 × 29 mm). Specimens D1 are similar to specimens C1, while specimens D2 are considerably longer. Specimens E1 are similar to specimen B3 and specimens E2 are similar to specimen B6.

Series D2 has a slenderness out of the limits given by the standard. It is used as a reference to observe the influence of second-order effects.

3. Results

3.1. Load-deformation behaviour

The results obtained from the compression tests are shown in Table 2. Figs. 5–7 show the load–displacement curves of series D, C, and F. The obtained curves are consistent with the three described behaviours by Dorn [5], as mentioned in Section 1:

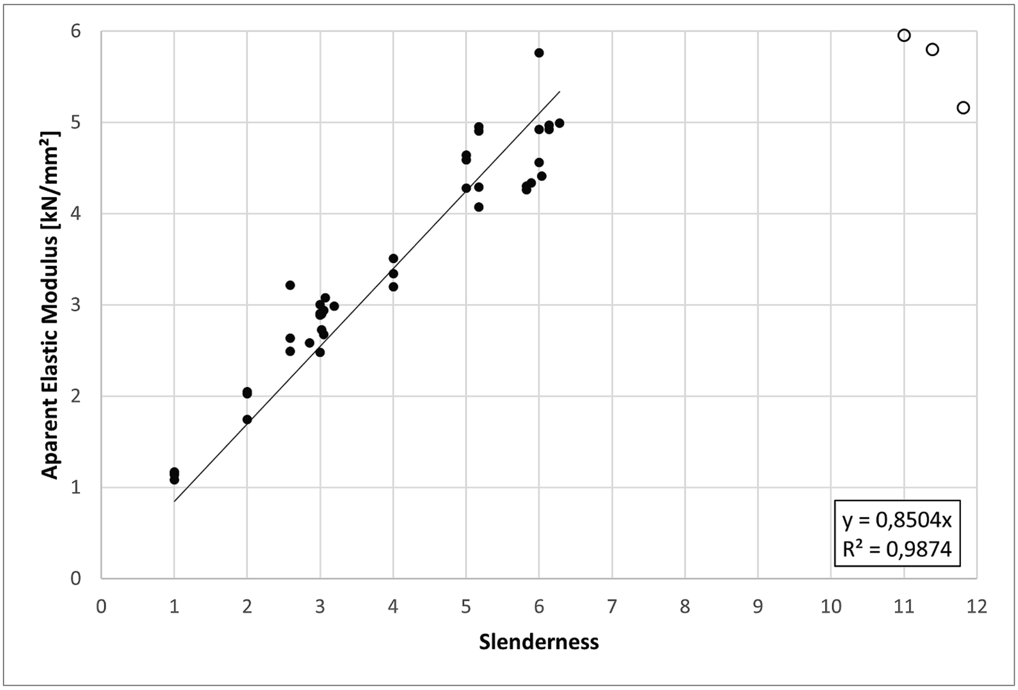

Fig. 3. Relationship between slenderness and the apparent modulus of elasticity from the initial loading between the 10 and 40% of F_{est}. Specimens with a slenderness over 10 are out of the tendency line.

- In the preloading phase, an initial adjustment zone may be seen in all specimens, which is followed by a zone of linear behaviour.
- Unloading phase: it may be clearly observed how the specimen undergoes a different way back, a sign of already existing plastic deformation. All specimens show an increase in the stiffness in the unloading phase.
- Loading phase: the loading stiffness is similar to the unloading stiffness in all specimens at least until the previously reached load. However, some specimens go back to the preloading stiffness of the specimens and others stay at the unloading stiffness.

3.2. Load–displacement stiffness

For each phase, the stiffness is calculated according to [6]:

$$K = \frac{(F_2 - F_1)}{(\delta_2 - \delta_1)} \tag{6}$$

where F_i is the applied force and δ_i is the corresponding displacement at two relevant points in the analysed loading phase. In the case of the initial loading phase, the initial point to obtain the stiffness was at 10% of the maximum capacity, not to take into account the initial adjustment. Linear fitting was additionally used to verify the obtained results for each range, with the same results and R^2 coefficients higher than 0.99 for most of the cases.

Table 2 shows the stiffness for the different preloading, unloading, and loading steps. As described above, an increase in the stiffness is noticed in the unloading phase. The unloading stiffness regarding the preloading stiffness has an increase of 24% for series A, 11% for series B, 32% for series C, 25% for series D, 27% for series E, and 27% for series F. The average increase of all series is 24% in comparison to the preload phase, with the maximum increase for specimen C2.3 (increase of 52%). Series B is the one with the lowest increase, from 8% in specimen B3 up to 14% in specimen B2.

Regarding the preloading phase, in comparison with the final loading phase, in the tests except in A2.1, the preloading stiffness is lower than the one for the loading phase, with an average reduction of 15%. The highest reduction is for specimen A1.2 with 33%. Specimen A2.1 is the only one that increases to 107%.

3.3. Apparent modulus of elasticity

For each specimen, the apparent elastic modulus (E_{app}), in which the axial stiffness of the specimen is considered, is calculated from the usual equation for axially loaded members as

$$E_{app} = \frac{L(F_2 - F_1)}{A(\delta_2 - \delta_1)} = \frac{L}{A}K \tag{7}$$

where L is the total height, F is the applied force, δ is the displacement, and A is the area of the cross section. This result, obtained in the loading phase, may be assumed as an apparent modulus of elasticity of the material, in which the geometrical influence of the specimen has already been taken into account. However, in this equation, the whole specimen is considered, and the effect of the contact area is incorporated. In the standard procedure, the modulus of elasticity is devised from the behaviour of the central part [6] (and it will be obtained below in Section 3.5).

In all tested series, it may be seen (Table 2) how this apparent elastic modulus increases as does the length of the specimen. As an example, in the series A, it varies from the minimum of 1 085 N/mm^2 for specimen A1.1 ($\lambda = 1$) to a maximum of 5 764 N/mm^2 for A6.1 ($\lambda = 6$). As shown in Fig. 3, a relation exists between this apparent elastic modulus and the slenderness of the specimen. A linear trend may be seen (with a correlation factor $R^2 = 0.85$), with only those specimens with a slenderness higher than 6 not following it. However, these latter are outside the limit given by the standard, and the presence of additional effects should be considered.

3.4. Strength

The strength of each specimen may be obtained as

$$f = \frac{F_{ult}}{A}, \tag{8}$$

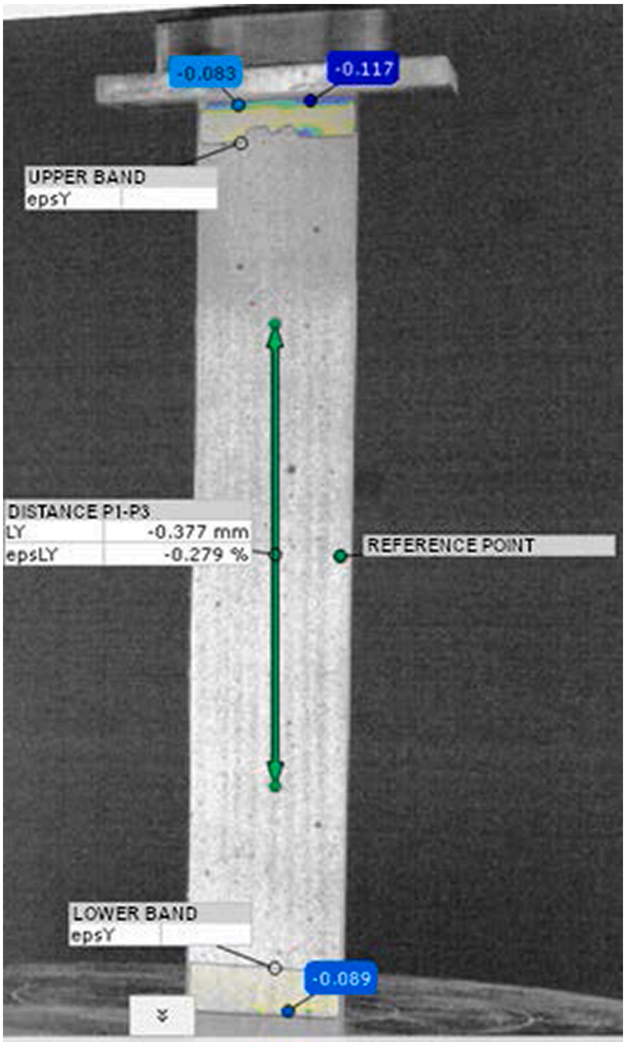

Fig. 4. One frame example of the Video Correlation analysis.

where F_{ult} is the maximum applied load, and A is the cross-section area of the specimen. The calculated strength for each specimen is given in Table 1. A consistent strength result is obtained within each series. Series A has a mean strength of 44,6 MPa, with a coefficient of variance of 6.2%, which is similar to the strength of series B (coming from the same timber member), which is 42,7 MPa (coefficient of variance 4.8%). Series D1, E, and F have a mean strength of 38,1 MPa and the coefficient of variation is 8.6%.

Such consistency of strength values within the series proves that no influence of second-order effects exists when the slenderness of the specimen is equal or lower than 6, as fixed by the standard. A reduction of the obtained strength is seen in series D2, whose slenderness is 11. As a conclusion, for those specimens with slenderness lower than 6, the obtained strength corresponds to that of the crushing of the material. This fact serves as a proof that any observed difference in the behaviour may be related to contact phenomena, and not to buckling issues.

3.5. Modulus of elasticity

As described above, the apparent modulus of elasticity (considering the whole specimen's length, described in Section 3.1) seems to increase with the length. However, such an apparent modulus considers the contact area, and it is thus not representative of the actual modulus of elasticity. According to the standard [6], to dismiss such influence of the contact interaction, the elastic modulus is measured in the central part of the specimen, within a distance four times the minor dimension of the specimen. The used equation is the same as (7), but where L is now the distance between the control points in the central zone, as shown in Fig. 4.

Obtained results are given in Table 2. The elastic modulus, when not considering the contact area, widely differs from the apparent elastic modulus. It is consistent throughout the test series, independently of the geometry, with a mean value of 12771 N/mm^2, and with a coefficient of variation of 18%. The obtained values are consistent with the characteristic (7400 N/mm^2) and mean (11000 N/mm^2) values given in EN338 [27] for C24 softwood. As a conclusion, the experimental elastic modulus confirms that the differences shown in the apparent elastic modulus do not refer to material differences, and may be thus related to contact phenomena.

4. Stiffness contact

As shown in the previous section, although the strength and modulus of elasticity prove how the specimens are quite similar, their elastic response relates to the slenderness of the specimen. This section analyses the hypothesis that such different behaviour is related to the contact interface, which may be modeled by means of the contact stiffness. As a result, it will propose an equation for its direct implementation into modeling software.

Other approaches, such as the modelling of the surfaces with their imperfections or adjusting the properties of the material of the surface according to the damage produced by the cutting tool, were discarded. Such approaches either require excessive modelling and computer cost, or make use of fictional material properties, which deem both inadequate for practice.

In the video correlation analysis, two stripes near the contact areas with higher deformation are observed. Fig. 4 shows the analysis of one frame of testing of one specimen as an example of how these stripes are visualized. The phenomena occurring in the contact interface may be assumed by a foundation modulus or contact stiffness, and it is proposed to model them as a strip of material with different elastic properties.

In all tested specimens, for any load, the observed deformation is higher than that obtained with the general elastic formulation for such a load with the Eq. (11). As a consequence, FE models tend to overestimate the stiffness [4,5]. This additional deformation due to the contact area could be considered by means of the stiffness contact SC, which is defined as the relationship between the pressure σ on the contact surface and the allowed overclosure $\delta_{(SC)}$ [14]:

$$SC = \frac{\sigma}{\delta_{(SC)}} \tag{9}$$

The total deformation may be obtained as

$$\delta = \delta_{(E)} + 2\delta_{(SC)} = \frac{FL}{EA} + 2\frac{\sigma}{SC}, \tag{10}$$

where $\delta_{(SC)}$ is the deformation of the contact area, and $\delta_{(E)}$ is that of the central part of the specimen, defined as

$$\delta_{(E)} = \frac{FL}{EA}. \tag{11}$$

From (10), SC may be obtained when assuming $\sigma = \frac{F}{A}$ and $K = \frac{F}{\delta}$, as

$$SC = \frac{2}{\left(\frac{A}{K} - \frac{L}{E}\right)} \tag{12}$$

where K is experimentally determined by Eq. (6) and E is the mean elastic modulus of wood [27].

Taking into account the stiffness contact parameter allows to consider an additional deformation in the specimens that simulates the

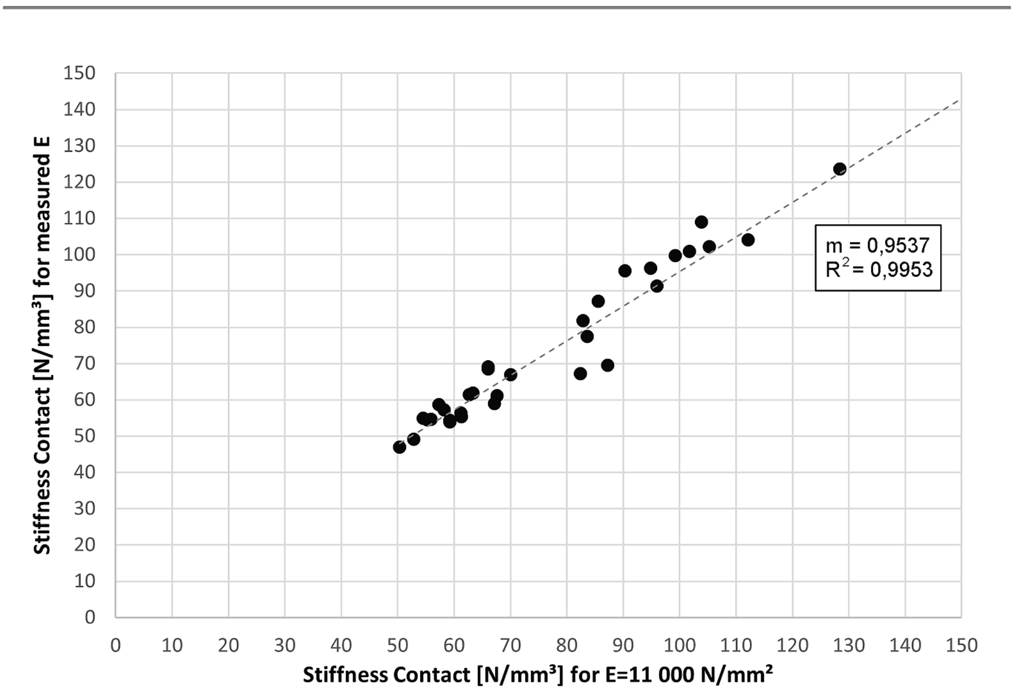

Fig. 8. Comparison of the obtained stiffness contact results when using the mean elastic modulus ($E = 11\,000\ \mathrm{N/mm^2}$) in comparison to the results obtained when the experimental elastic modulus is considered.

different behavior of the contact surfaces. This phenomenological parameter that simulates the micromechanics happening in the surface and the nearest zones.

The obtained values for each specimen are shown in Table 2. It is shown how the stiffness contact value varies from the lowest 50 N/mm^3 for specimen C1.2 to 161 N/mm^3 for specimen A6.1. The mean value for the specimens is 82 N/mm^3 with a coefficient of variation of 30%. The obtained stiffness contact values, SC_E, given in Table 2, are quite consistent among the different series, which shows how the contact interaction may be assumed as the parameter explaining the observed change in apparent stiffness. The series A is the one with the highest coefficient of variation with 31%, with stiffness contact values starting in 86 N/mm^3 for specimen A3.1 up to 161 N/mm^3 for specimen A6.1, it is remarkable that this series has a slenderness from 1 to 6. On the other hand, series B has a mean value of 61 N/mm^3 with a coefficient of variation of 10%. For series C1, C2, D1, D2, E1, E2, and F1, the coefficients of variation are 16%, 19%, 4%, 15%, 10%, 11% and 7% respectively showing that not big dispersion is achieved inside the series in contrast with the dispersion obtained for all series simultaneously at the 30%.

Since obtaining the actual elastic modulus for each specimen would deem not feasible in common practice, the stiffness contact may be obtained from (12), but using the mean elastic modulus given in the standard for the corresponding strength class instead of the actual one.

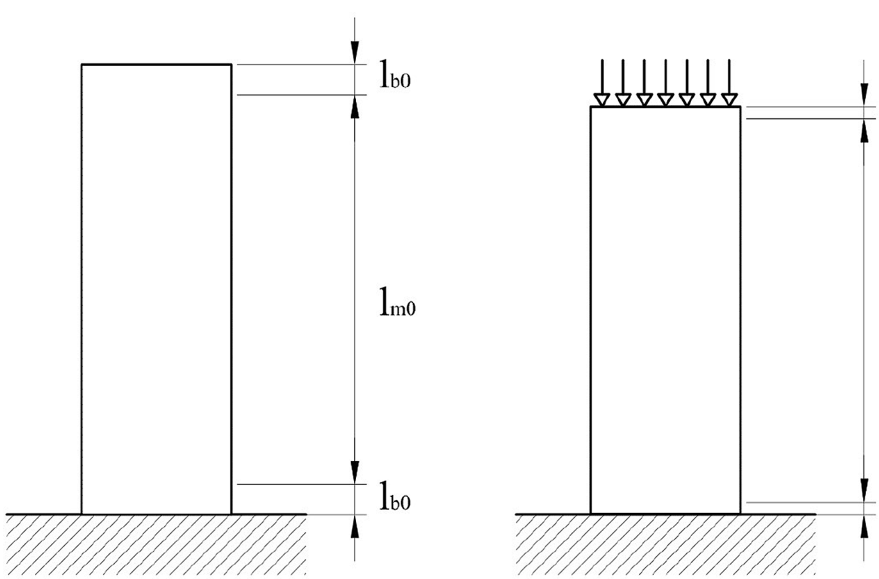

Fig. 9. Theoretical model for the stiffness contact calculation Iraola [30]. Subindex 0 refers to the initial state, previous to the load, and subindex 1 refers to the lengths when loaded.

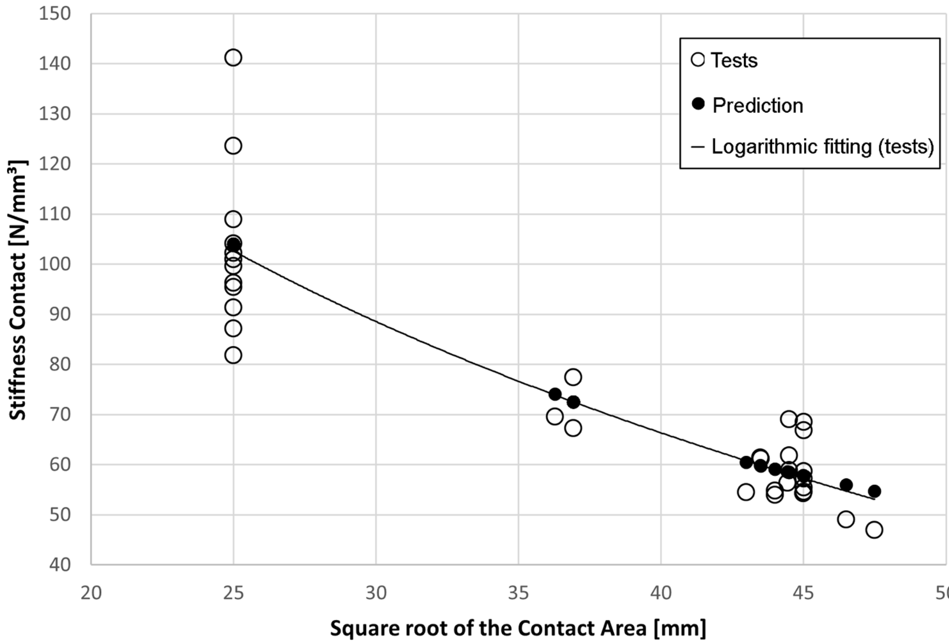

Fig. 10. Adjustment of the stiffness contact equation to the analytically obtained with the mean and measured Elastic Modulus.

The obtained value when the elastic modulus from the standard is considered, SC_{11}, is given in Table 2. Fig. 8 compares the obtained stiffness contact results when using the mean elastic modulus from the standard (SC_{11}) in comparison to the results obtained when the experimental elastic modulus (SC_E) for each specimen is considered. As shown, small differences are obtained, being the fitting slope close to one and with a coefficient of correlation R^2 higher than 0.99. Therefore, for practical reasons, the use of the mean elastic modulus may be deemed as sufficient.

4.1. Alternative analytical methods

Some alternative analytical models may be found in literature. A spring model was developed by Cepelka and Malo [10] to account for the effects of contact in wood. It simulates the stiffness of the wood with a spring and adds an additional spring for each contact area, resulting in a series spring model, where the inverse of the total stiffness value is obtained according to

$$\frac{1}{K_{total}} = \frac{1}{K_{wood}} + 2\frac{1}{K_{layer}}. \tag{13}$$

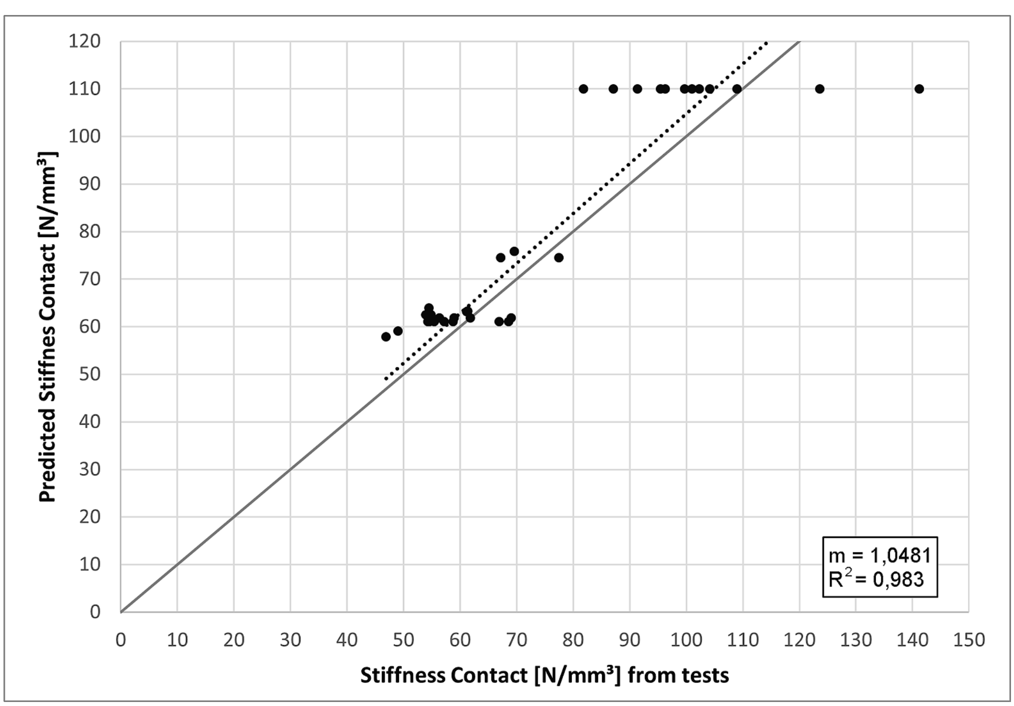

Fig. 11. Comparison of predicted stiffness contact with Eq. (15) with the experimental stiffness contact values. The ideal correlation line $y = x$ is plotted for comparison purposes.

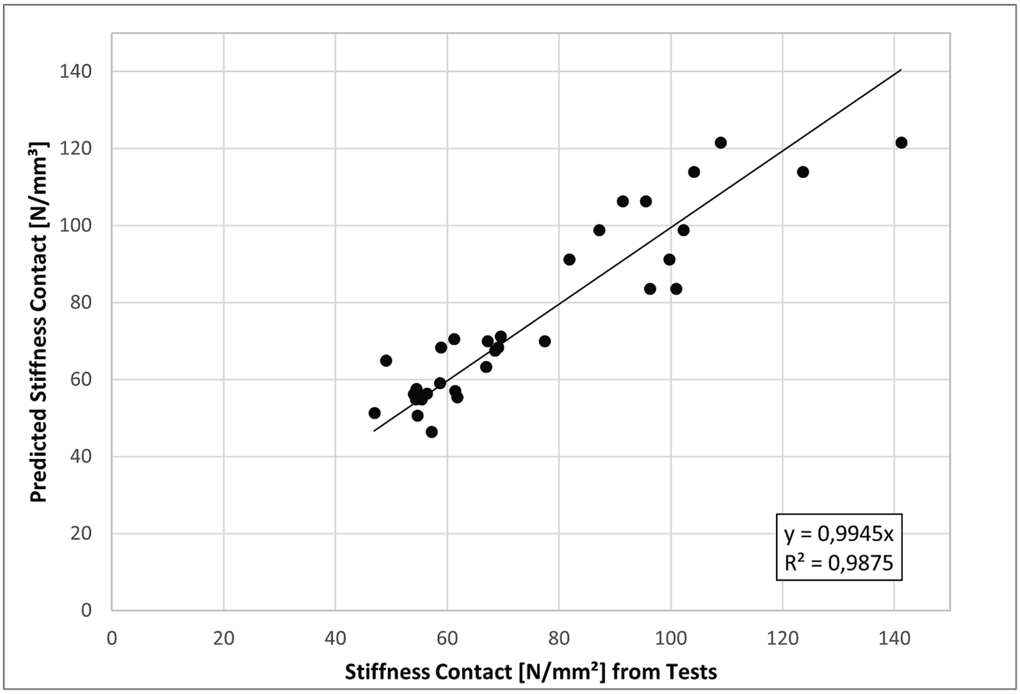

Fig. 12. Comparison of the obtained stiffness contact when additionally the slenderness of the specimen (16). is considered.

A very similar method was proposed by Iraola [30] to account for the contact area behaviour, where the contact is simulated by an additional material (with a different elastic modulus, E_b) located as a band in the contact area. The model is shown in Fig. 9, where ℓ_{b0} is the thickness of each layer and ℓ_{m0} is the height of the specimen minus the thickness of these two layers. By applying the usual equations for axial deformation, the elastic modulus of the additional "contact" material may be calculated from the experimental E_{app}

$$\frac{\ell}{E_{app}} = \frac{\ell_{m0}}{E} + 2\frac{\ell_{b0}}{E_b}, \tag{14}$$

where $\ell = \ell_{m0} + 2\ell_{b0}$.

These alternative methods obtain the same results as those from (12), as they are just different expressions of the same physical problem. From the Eqs. (13) and (14), it is possible to obtain the values for the SC parameter, what seems to be the best way to face the problem not having to develop a model with springs or additional material bands.

4.2. Proposal for practical implementation

With the above experimental procedure and analysis, a very precise stiffness contact parameter may be obtained. However, the required data is not available in common practice. As a first step, it was previously demonstrated how using the standard mean elastic modulus deemed in minimal variation on the predicted results (see Fig. 8). In this section, an equation which allows to obtain the required stiffness contact in the modeling phase, based only on the geometry of the specimens, is proposed.

The proposed equation has been developed under consideration in the literature (see Section 1) that the contact area mostly influences the contact response, and how in previous proposals (which dealt with cylindrical contact) such area is accounted as $\sqrt{A}$. Apart from the area, a fitting parameter is introduced:

$$SC_{cal,A} = 1\,300\left(\frac{a+b}{ab}\right) = \frac{2\,600}{\sqrt{A}} \tag{15}$$

where a and b are the sides of the rectangular cross-section in contact and A is the area.

Fig. 10 shows the good adjustment of the equation to the trendline of the analytically obtained values ($SC_{cal,A}$, black-filled) and Fig. 11 shows the comparison among the values obtained with (15) ($SC_{cal,A}$) and the experimental ones (SC_E) for each specimen. As shown by the fitting line, the equation obtains a remarkable similar performance, with a determination coefficient $R^2 = 0,983$. The obtained SC_{cal} for each specimen shows a good relation with the SC calculated with the mean values of each series with the Eq. (12) as it is shown in Figs. 10 and 11. Moreover, the obtained value is similar to the stiffness contact of 115 N/mm^3 for steel-wood contact in the parallel direction applied by Kekeliak et al. [31].

Due to the fact that the experimental campaign was limited to C24 softwood, it is assumed that (15) is only adequate for that strength class. The required numerical fitting parameters may be obtained for different wood species and strength classes by following the experimental and analytical procedures explained above. Eq. (15) is similar to Eq. (1) [7,15], which was developed for cylindrical contact. If (1) is modified to consider the applied pressure instead of the load (by dividing the force F by the area A) so that it follows the above presented definition of stiffness contact, then it becomes

$$SC_{ind}\frac{1}{A} = \frac{2}{\sqrt{\pi}}\sqrt{A}E_r\frac{1}{A} = \frac{2E_r}{\sqrt{\pi}}\frac{1}{\sqrt{A}}, \tag{(1)'}$$

which proves that when the stiffness contact is defined as the pressure-overclosure relation, the previously reported area influence shows an inverse relation and thus, appears in the denominator. The fitting parameter in (15) may be assumed as being related to the geometry of the contact area and the modulus of elasticity of timber.

In Figs. 10 and 11, several outliers may be spotted for the calculated stiffness contact of 104 N/mm^3. Since the Eq. (15) only requires the area of the specimen, the same value is obtained for those specimens with the same area. However, an influence of the slenderness may be observed, especially in the series A ($\sqrt{A}$ = 25mm). The slenderness could be included as an additional parameter to obtain a better fit to the experimental results

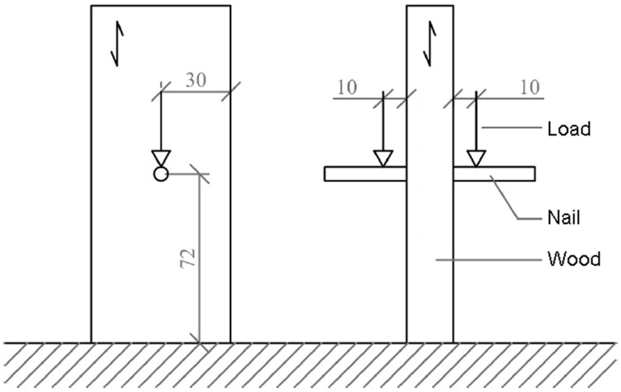

Fig. 13. Embedment test series configuration.

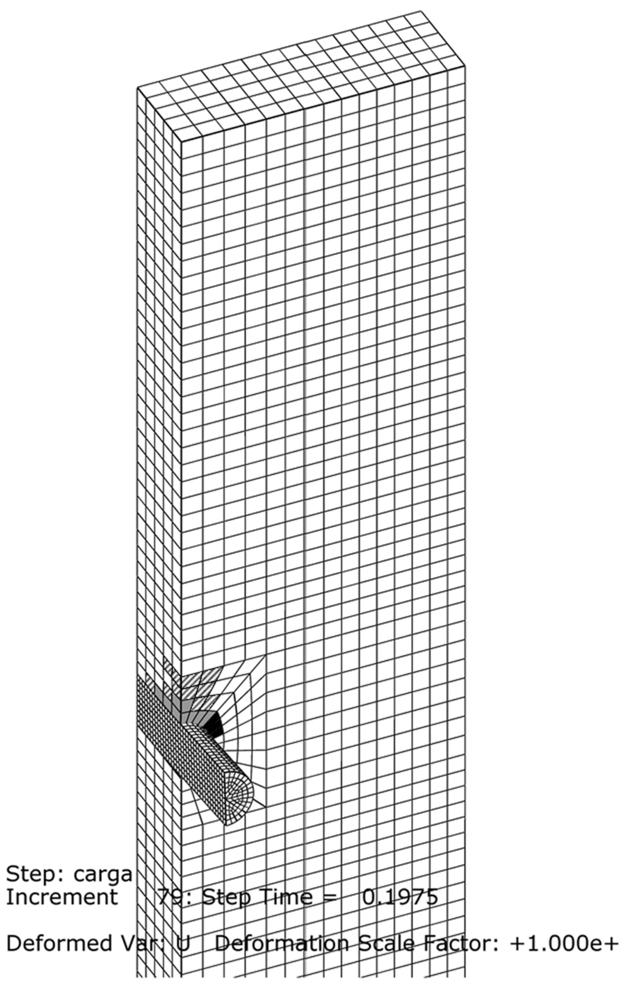

Fig. 14. FE model geometry visualization. Black elements show failure due to compression in the direction perpendicular to the fibers, stripped elements show failure due to compression in the direction of the fibers and gray elements show a combination of failure types.

$$SC_{cal,B} = 1\,900\left(\frac{0,1\lambda + 1}{\sqrt{A}}\right). \tag{16}$$

The resulting performance is enhanced, as shown in Fig. 12 and in Table 2 ($SC_{cal,B}$). However, this latter equation including the slenderness of the specimen becomes of difficult practical application for cases different to the axial load used in the experimental procedure. Therefore, (15) is preferred for practical purposes.

5. Application

5.1. Embedment test

Iraola [30] used a simple embedment test to improve the simulation in FE-models of dowel-type fasteners connections in timber. The test configuration is shown in Fig. 13, where 6 mm diameter nails were pushed into a wood specimen with a cross section of 20 × 60 mm and a length of 144 mm.

A FE-model was developed in ABAQUS [14] implementing cohesive elements defined by Dourado et al. [32] and user subroutines with the material script developed by Iraola and Cabrero [33] to simulate the failure behaviour. Different mechanical properties for each direction and for tension and compression were considered along with progressive failure and element elimination. However, these techniques have no influence on the resultant stiffness of the joint defined between 10% and 40% of the ultimate load [6].

Fig. 14 shows the main geometry and the resulting progressive failure of the FE model with two planes of symmetry. The vertical displacement and the rotation of the base are constrained. A vertical displacement is applied in the loading area of the nail, which is modelled with a mesh that makes the nodes of the nail and the wood concur. The contact behaviour in the normal direction for the timber-to-steel interface was defined by a linear pressure-overclosure relationship, with a slope SC_{cal} obtained in Eq. (15). For the tangential direction a penalty friction formulation with a friction coefficient of 0.3 [34] was used. Black elements show failure due to compression in the direction perpendicular to the fibers, stripped elements show failure due to compression in the direction of the fibers, and gray elements show a combination of failure types.

The stiffness contact parameter defined in Eq. (15) implemented in the FE-model improves the simulation of the stiffness of the joint. Parameters a and b of Eq. (15) were defined as the width of the wood member and the diameter of the dowel, respectively.

Fig. 15 shows the experimental results in comparison with the FEA simulation with and without the stiffness contact parameter. According to [6], the experimental results show a mean stiffness of 3918 N/mm with a coefficient of variation of 8.8%, whereas the FEM with the Hard Contact shows a stiffness of 6097 N/mm, 156% of the experimental stiffness. Implementing the stiffness contact parameter of Eq. (15) results in a stiffness of 4641 N/mm, 118% of the experimental stiffness. As shown in the results, in this particular test, a high variability of the experimental response is observed, corresponding the model response to the most stiff experimental one.

5.2. Moment transmitting joint

The stiffness contact calculated with Eq. (15) (SC_{cal}) was implemented in the modelling of a series of moment transmitting joints of different geometries. The FEM software ABAQUS [14] was again used and the required stiffness contact parameter was defined with Eq. (15). The script developed by Iraola and Cabrero [33] was used to model the fracture behaviour of timber.

The obtained results were validated with an experimental campaign, one of whose specimens is shown in Fig. 17. The joint consists of two parallel C24 column members to which a central C24 beam is attached by means of eight steel dowels. Parameters a and b of Eq. (15) were defined as the width of the wood member and the diameter of the dowel, respectively.

Fig. 16b shows the main geometry and boundary conditions of the FE model with one plane of symmetry. The displacements of both extremes of the column are constrained, while the rotations are allowed. Since the implemented user subroutine [33] modifies the properties of each element, the FE model is therefore mesh-dependent. Each part was

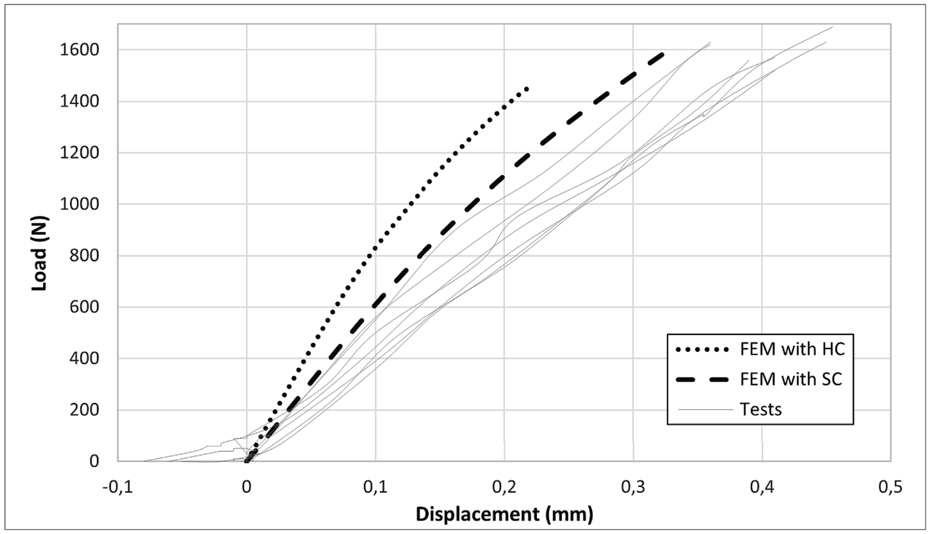

Fig. 15. Experimental results of the preloading step in comparison with FEA with Hard Contact and stiffness contact approaches. Experimental data has been displaced to concur in the origin, discarding initial adjustments.

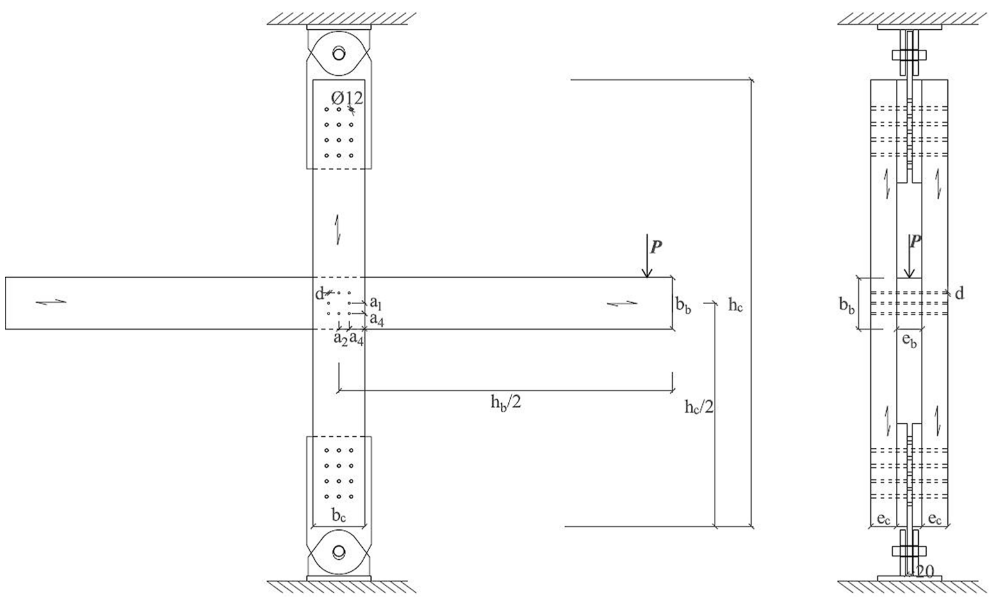

Fig. 17. Moment transmitting connection used for application [35].

partitioned and meshed to obtain the most homogeneous element distribution close to the contact zone (see Fig. 16a). The contact behaviour in the normal direction for the timber-to-steel interface was defined by a linear pressure-overclosure relationship, with a slope SC_{cal} obtained in Eq. (15). For the tangential direction a penalty friction formulation with a friction coefficient of 0.3 [34] was used.

Fig. 18 shows the experimental results of three tests in comparison to the FEM simulation with and without the stiffness contact parameter. The F_{est} of the first tested joint was overestimated resulting in an unloading path starting over the 1,5 kN mark, the F_{est} was afterwards adjusted for the remaining tests. The model does not account for the initial plastification, therefore the unloading and reloading paths fit the original path and the unloading is omitted in the model.

A good agreement with the experimental results is obtained when the stiffness contact parameter is considered, while not considering such contact phenomena results in an overprediction of the stiffness of the joint.

For a complete description of the experimental campaign and the used modeling techniques, the reader is referred to Basterrechea-Arevalo et al. [35].

6. Conclusions

Modelling the contact behaviour of wood members is a challenge due to the heterogeneity and complexity of the material. Especially in the case of wood joints, their elastic response cannot be accurately modelled without considering the singularities of the contact areas. The stiffness contact parameter included in some FEA software allows researchers to introduce some of those singularities in a simple way, by means of a contact stiffness parameter. Although the initial adjustment behaviour is not considered in this parameter, the behaviour after this initial zone can be precisely simulated.

Since the determination of the stiffness contact parameter requires data only available through testing, an alternative method to determine it for C24 softwood (being this the typical one in Europe) is proposed. By developing further experimental campaigns, this equation could be

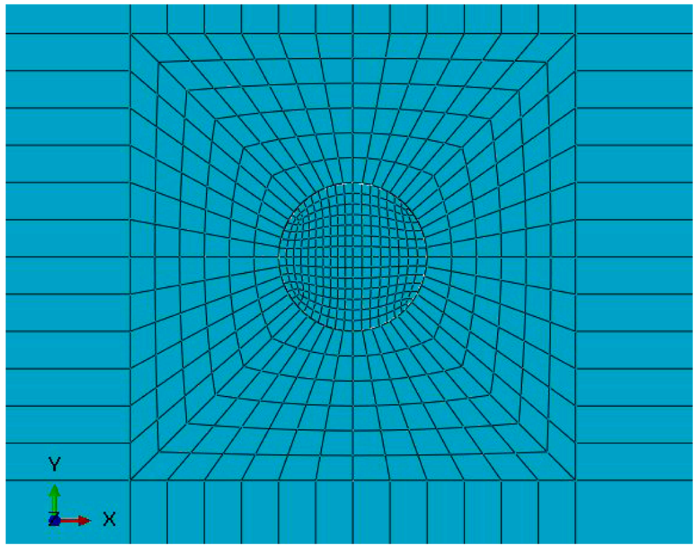

(a) Mesh for the contact zone.

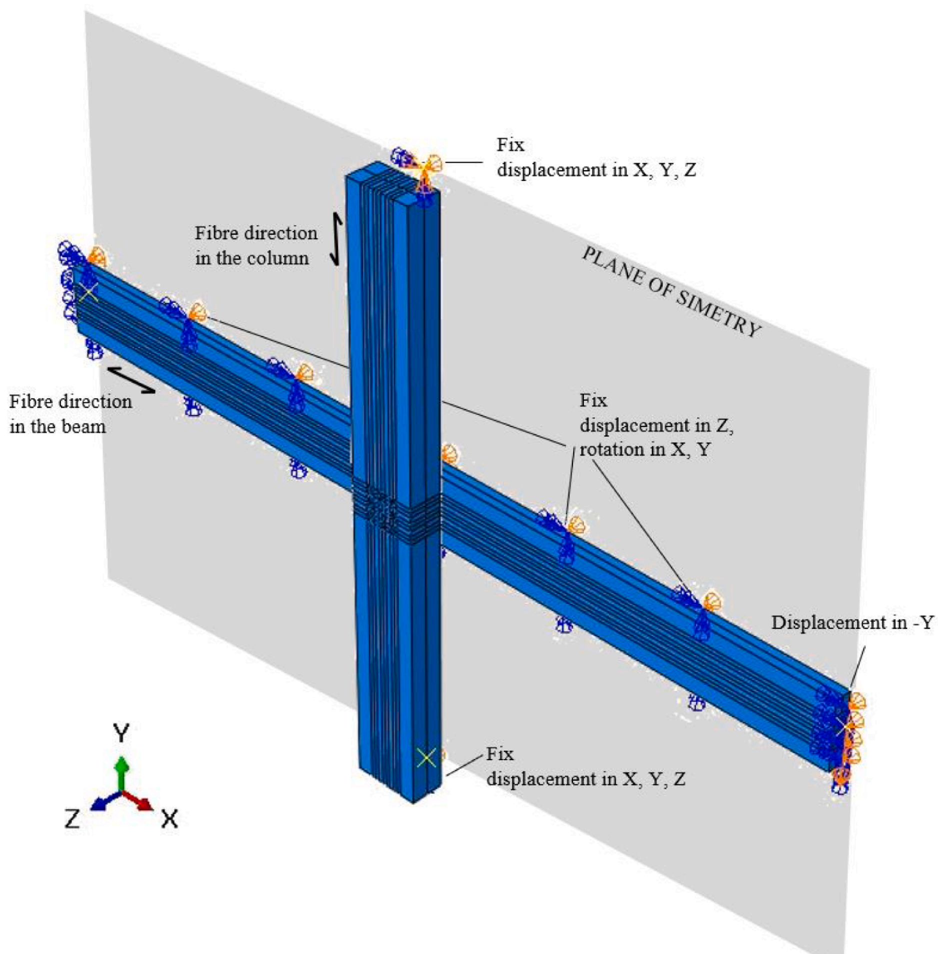

(b) Outline and boundary conditions.

Fig. 16. Details of the FE-model of moment transmitting beam-to-column connection [35].

expanded for alternative wood species. The proposed determination method is based only on the geometry of the contact area and seems to be able to accurately predict the behaviour of rectangular contact areas for such a heterogeneous and variable material as wood.

No correlation was achieved studying the slenderness of each specimen. Upcoming research will further study this point and the influence of the wood mean elastic modulus to see if the factor in the Eq. (15) may be related to the mean elastic modulus or not.

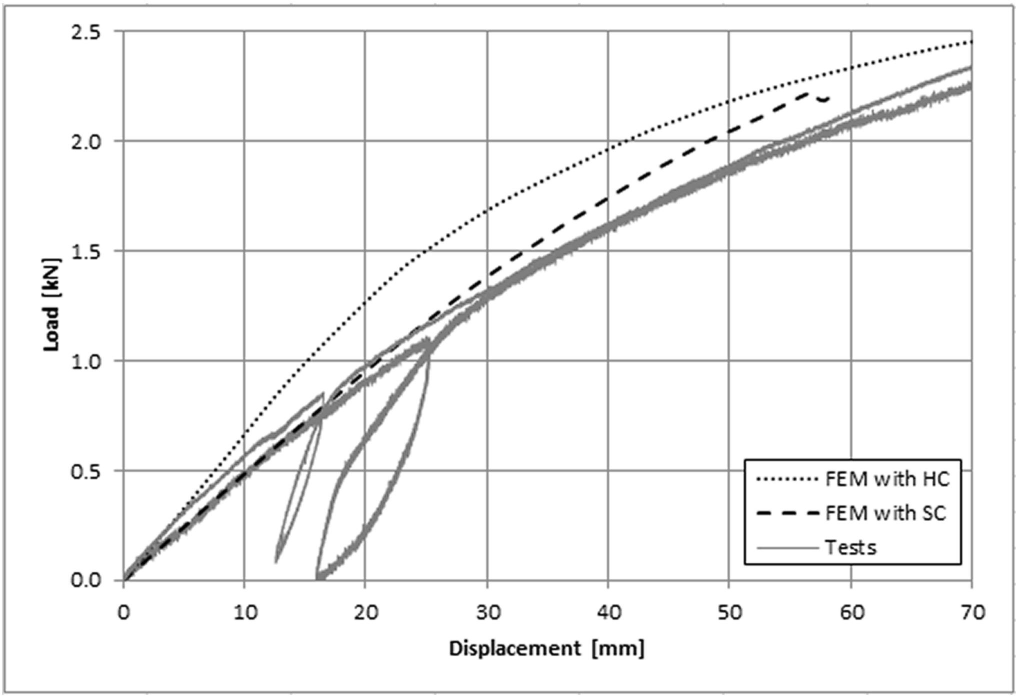

Fig. 18. Application of the derived contact stiffness formula to the modeling of a moment transmitting connection [35].

Declaration of Competing Interest

The authors declare that they have no known competing financial interests or personal relationships that could have appeared to influence the work reported in this paper.

Acknowledgements

The financial support provided by the Spanish Ministerio de Economía y Competitividad and Fondo Europeo de Desarrollo Regional under contract BIA2016-80358-C2-1-P MINECO/FEDER UE is gratefully acknowledged. The help provided to the third author by the Friends of the University of Navarra Association for her PhD is greatly recognised as well.

References

[1] Kuzmanovska I, Gasparri E, Monne DT, Aitchison M. Tall timber buildings: Emerging trends and typologies. In: WCTE 2018 - World Conference on Timber Engineering; August 2018.
[2] Ramage M, Foster R, Smith S, Flanagan K, Bakkar R. Super Tall Timber: design research for the next generation of natural structure. J Archit 2017;22(1):104–22.
[3] EN-26891, Timber structures–joints made with mechanical fasteners. General principles for the determination of strength and deformation characteristics; 1991.
[4] Sandhaas C. Mechanical behaviour of timber joints with slotted-in steel plates, Ph. D. thesis, Technische Universiteit Delft; 2012.
[5] Dorn M. Investigations on the serviceability limit state of dowel-type timber connections: Untersuchungen zum Gebrauchstauglichkeitszustand von Dübelverbindungen im Holzbau, Ph.D. thesis; 2012.
[6] EN-408, Timber structures - Structural timber and glued laminated timber - Determination of some physical and mechanical properties, CEN; 2012.
[7] Pharr G, Oliver W, Brotzen F. On the generality of the relationship among contact stiffness, contact area, and elastic modulus during indentation. J Mater Res 1992;7(3):613–7.
[8] Cheng Y-T, Cheng C-M. General relationship between contact stiffness, contact depth, and mechanical properties for indentation in linear viscoelastic solids using axisymmetric indenters of arbitrary profiles. Appl Phys Lett 2005;87(11):111914.
[9] ASTM-D143, Standard test methods for small clear specimens of timber, West Conshohocken, PA, USA: ASTM International.
[10] Cepelka M, Malo KA. Experimental study of end grain effects in timber joints under uniaxial compression load. In: Proceedings of world conference on timber engineering (WCTE 2016); 2016.
[11] Kiwelu HM. Experimental study on the effect of moisture on bolt embedment and connection loaded parallel to grain for timber structures. Tanzania J Eng Technol, 38.
[12] Kiwelu H, Smith I, Asiz A, Finite element models of effects of moisture on bolt connection properties of GLULAM. In: World Conference on Timber Engineering (WCTE 2014); 2014.
[13] Hong J-P, Barrett D. Three-dimensional finite-element modeling of nailed connections in wood. J Struct Eng 2010;136(6):715–22.
[14] Abaqus, 6.14 Documentation, Dassault Systemes Simulia Corporation 2014;651: 6–2.
[15] Yang F. Contact stiffness of initially stressed neo-Hookean solids. J Polym Sci, Part B: Polym Phys 2004;42(13):2513–21.
[16] Pietrement O, Troyon M. General equations describing elastic indentation depth and normal contact stiffness versus load. J Colloid Interface Sci 2000;226(1): 166–71.
[17] Hahn J. Durchlaufträger, Rahmen, Platten und Balken auf elastischer Bettung, Werner; 1970.
[18] Eisenberger M, Yankelevsky DZ. Exact stiffness matrix for beams on elastic foundation. Comput Struct 1985;21(6):1355–9.
[19] Mirdad MAH, Chui YH. Stiffness prediction of Mass Timber Panel-Concrete (MTPC) composite connection with inclined screws and a gap. Eng Struct 2020;207: 110215.
[20] Reynolds T, Harris R, Chang W-S. An analytical model for embedment stiffness of a dowel in timber under cyclic load. Eur J Wood Wood Prod 2013;71(5):609–22.
[21] Lekhnitskii SG. Anisotropic plates, Tech Rep, Foreign Technology Div Wright-Patterson Afb Oh; 1968.
[22] Zhang K-D, Ueng CE. Stresses around a pin-loaded hole in orthotropic plates. J Compo Mater 1984;18(5):432–46.
[23] Yurrita M, Cabrero JM. Effective thickness of timber elements for the evaluation of brittle failure in timber-to-steel connections with large diameter fasteners loaded parallel-to-grain at the elastic range: A new method based on a beam on elastic foundation. Eng Struct 2020;209:109959.
[24] Lemaitre R, Bocquet JF, Schweigler M, Bader TK. Beam-on-Foundation (BOF) Modelling as an Alternative Design Method for Timber Joints with Dowel-Type Fasteners – Part 1: Strength and Stiffness per Shear Plane of Single-Fastener Joints. In: International Network on Timber Engineering (INTER), Paper 51–7–13; 2018.
[25] Lemaitre R, Bocquet JF, Schweigler M, Bader TK. Beam-on-foundation modelling as an alternative design method for timber joints with dowel-type fasteners – Part 4: Joints Subjected to In-Plane Loading. In: International Network on Timber Engineering (INTER), Paper 53–7–4; 2020.
[26] Hwang K Komatsu K. Bearing properties of engineered wood products I: Effects of dowel diameter and loading direction. J Wood Sci 2002;48(4): 295–301, ISSN 14350211, doi:10.1007/BF00831350.
[27] EN-338, Structural Timber - Strength classes, CEN; 2016.
[28] EN-1912, Structural Timber - Strength classes - Assignment of visual grades and species, CEN; 2010.
[29] GOM Correlate Professional, Digital Image Correlation and Strain Computation Basics, GOM GmbH, 38122 Braunschweig Germany, 2016.

[30] Iraola B. Simulación del comportamiento mecánico de la madera en uniones estructurales y su aplicación mediante modelos tridimensionales de elementos finitos., Ph.D. thesis, Universidad de Navarra; 2016.
[31] Kekeliak M, Gocál J, Vičan J. Stiffness of Carpentry Connections-Numerical Modelling vs. Experimental Test. Civil Environ Eng 2015;11(2):121–35.
[32] Dourado N, Morel S, De Moura M, Valentin G, Morais J. Comparison of fracture properties of two wood species through cohesive crack simulations. Compos Part A: Appl Sci Manuf 2008;39(2):415–27.
[33] Iraola B, Cabrero J. An algorithm to model wood accounting for different tension and compression elastic and failure behaviors. Eng Struct 2016;117:332–43.
[34] Gečys T, Daniunas A, Bader TK, Wagner L, Eberhardsteiner J. 3D finite element analysis and experimental investigations of a new type of timber beam-to-beam connection. Eng Struct 2015;86:134–45. https://doi.org/10.1016/J.ENGSTRUCT.2014.12.037. ISSN 0141–0296.
[35] Basterrechea-Arevalo M, Cabrero J, Iraola B, Goñi R. Moment transmitting beam-to-column timber connections: finite element modelling and experimental validation; 2021.